Numer. Math. Theor. Meth. Appl.
doi: 10.4208/nmtma.2011.m1036

Vol. 4, No. 4, pp. 576-597
November 2011

High Order Scheme for Schrödinger Equation with Discontinuous Potential I: Immersed Interface Method

Hao Wu*

Department of Mathematical Sciences, Tsinghua University, Beijing, 10084, China.

Received 22 October 2010; Accepted (in revised version) 21 March 2011

Available online 7 November 2011

Abstract. The immersed interface method is modified to compute Schrödinger equation with discontinuous potential. By building the jump conditions of the solution into the finite difference approximation near the interface, this method can give at least second order convergence rate for the numerical solution on uniform cartesian grids. The accuracy of this algorithm is tested via several numerical examples.

AMS subject classifications: 35R05, 65M06, 81Q05

Key words: Schrödinger equation, discontinuous potential, immersed interface method, finite difference method.

1. Introduction

Consider Schrödinger equation in different forms

$$\text{Stationary}: \quad -\tfrac{1}{2}\varepsilon^2\triangle\varphi + V\varphi = E\varphi, \tag{1.1}$$

$$\text{Eigenvalue}: \quad -\tfrac{1}{2}\varepsilon^2\triangle\phi + V\phi = E\phi, \tag{1.2}$$

$$\text{Dynamic}: \quad i\varepsilon\psi_t + \tfrac{1}{2}\varepsilon^2\triangle\psi = V\psi, \tag{1.3}$$

where ε is the re-scaled Plank constant, $\boldsymbol{x} \in \Omega \subset \mathbb{R}^d$ denotes the computational domain, and $V = V(\boldsymbol{x})$ is the potential. We can use different types of boundary conditions, e.g., transparent boundary condition, periodic boundary condition and reflection boundary condition. In the stationary problem, the energy E is specified. In the eigenvalue problem, the energy E is eigenvalue. In the dynamic problem, we need to specify the initial condition as

$$\psi(0,\boldsymbol{x}) = A_0(\boldsymbol{x})e^{\frac{iS_0(\boldsymbol{x})}{\varepsilon}}. \tag{1.4}$$

Our goal is to compute the wave functions $\varphi(\boldsymbol{x})$, $\phi(\boldsymbol{x})$ and $\psi(t,\boldsymbol{x})$ on a uniform Cartesian grid up to second order accuracy, even if the discontinuities curves of potential $V(\boldsymbol{x})$ are not aligned with the grid.

*Corresponding author. *Email address:* hwu@tsinghua.edu.cn (H. Wu)

Schrödinger equation with discontinuous potential can be used to model motion of electrons in quantum zones, e.g., quantum barrier, quantum well, quantum dot and p-n junctions [11, 30, 37]. The quantum zone is an active region of electronic structure, which connects to two highly conduct large reservoirs. The whole structure is a basic and fundamental semiconductor device in modern industry, e.g., memory chip, microprocessor and integrated circuit [9, 10, 31].

There have been numerous studies on direct numerical methods of Schrödinger equation, including the finite difference method [28,29,38], the discontinuous Galerkin method [26, 27, 40], spectral type methods [7, 8, 13], the WKB scheme [3, 4, 36] and other related technics [1, 2, 5, 17, 34]. However, none of these methods could satisfy all the following requirements for solving Schrödinger equation with discontinuous potential: (i) at least second order convergence, (ii) robust processing in interface conditions, (iii) easy generalization to high dimensions, (iv) taking the advantages of the Cartesian grid.

The immersed interface method, originally developed for elliptic equations with discontinuous coefficients and singular sources [12, 18, 20–24], can maintain at least second order accuracy on a uniform grid even when the discontinuities curves of potential are not aligned with the grid. The idea is to modify the standard finite difference approximation at grid points near the interface to keep jump conditions of solutions' derivatives. Such method has succeed in many applications, e.g., the heat equation [6, 25], the acoustic wave equation [33, 41], stokes flow and Navier-Stokes equations [15, 16, 19].

In this paper, we develop an immersed interface method to solve Schrödinger equation with discontinuous potential. The solutions are shown to have at least second order convergence in both one and two dimensions. A more interesting question is how to extend such idea for the dynamic Schrödinger equation with discontinuous potential in the semi-classical regime [14]. Based on the results here, we will propose two new methods in a consecutive paper [39].

The paper is organized as follows. In Section 2, we show how the immersed interface method is applied to Schrödinger equation with discontinuous potential. The method in higher space dimensions is given in Section 3. In Section 4, we present numerical examples to test the accuracy of the method. We make some conclusive remarks in Section 5.

2. One dimensional Schrödinger equation

We begin by considering the one dimensional stationary Schrödinger equation

$$-\frac{1}{2}\varepsilon^2\varphi_{xx} + V\varphi = E\varphi, \tag{2.1}$$

on the computational domain $[a, b]$. The potential $V(x)$ is split into a smooth part $V_s(x) \in C^\infty([a, b])$ and a discontinuous part $V_d(x)$

$$V(x) = V_s(x) + V_d(x). \tag{2.2}$$

Here the discontinuous potential is given by

$$V_d(x)=\begin{cases}\Lambda, & c_1<x<c_2,\\ 0, & \text{else.}\end{cases} \tag{2.3}$$

Remark 2.1. The discontinuous potential $V_d(x)$ can be considered in a general form, including more discontinuities. To concentrate on the key idea, we use (2.3) in this Section without any special instructions.

Therefore, we have the following jump conditions ($s=1,2$):

$$\begin{cases}[V]_{c_1}=\Lambda, \quad [V]_{c_2}=-\Lambda,\\ \left[\varphi\right]_{c_s}=0, \quad \left[\varphi_x\right]_{c_s}=0,\\ -\dfrac{1}{2}\varepsilon^2\left[\varphi_{xx}\right]_{c_s}+[V]_{c_s}\varphi^{c_s}=0.\end{cases} \tag{2.4}$$

Here $[\cdot]_c$ represents the jump in a quantity at the point c

$$\left[\varphi\right]_c=\varphi^{c^+}-\varphi^{c^-}=\lim_{x\to c^+}\varphi(x)-\lim_{x\to c^-}\varphi(x).$$

We would like to compute the numerical solution of $\varphi(x)$ on a uniform grid

$$x_n=nh+a, \quad n=0,1,\cdots,N,$$

where $h=(b-a)/N$. The point c_s will typically fall between grid points, say

$$x_{m_s}\le c_s\le x_{m_s+1}.$$

We introduce $p_{s1},p_{s2}\in[0,1]$ such that

$$p_{s1}+p_{s2}=1, \quad c_s-x_{m_s}=p_{s1}h, \quad x_{m_s+1}-c_s=p_{s2}h.$$

For $n\neq m_s,m_s+1$, the solution is smooth in the interval $[x_{n-1},x_{n+1}]$, and we can use the standard approximation

$$-\frac{1}{2\tau^2}\left(\varphi^{n-1}-2\varphi^n+\varphi^{n+1}\right)+V^n\varphi^n=E\varphi^n, \tag{2.5}$$

where $\tau=h/\varepsilon$. This gives a local truncation error

$$T^n=-\frac{1}{2}\frac{\varepsilon^2}{h^2}\left(\varphi^{n-1}-2\varphi^n+\varphi^{n+1}\right)+V^n\varphi^n-E\varphi^n=\mathcal{O}(h^2).$$

To design the finite difference scheme at $n=m_s$, we firstly have

$$\begin{aligned}\varphi(x_{m_s-1})=&\varphi^{c_s}-(p_{s1}+1)h\varphi_x^{c_s}+\frac{1}{2}(p_{s1}+1)^2h^2\varphi_{xx}^{c_s^-}+\mathcal{O}(h^3),\\ \varphi(x_{m_s})=&\varphi^{c_s}-p_{s1}h\varphi_x^{c_s}+\frac{1}{2}p_{s1}^2h^2\varphi_{xx}^{c_s^-}+\mathcal{O}(h^3),\\ \varphi(x_{m_s+1})=&\varphi^{c_s}+p_{s2}h\varphi_x^{c_s}+\frac{1}{2}p_{s2}^2h^2\varphi_{xx}^{c_s^+}+\mathcal{O}(h^3)\\ =&\varphi^{c_s}+p_{s2}h\varphi_x^{c_s}+\frac{1}{2}p_{s2}^2h^2\left(\varphi_{xx}^{c_s^-}+\frac{2[V]_{c_s}}{\varepsilon^2}\varphi^{c_s}\right)+\mathcal{O}(h^3),\end{aligned}$$

and

$$\begin{aligned}&V(x_{m_s})\varphi(x_{m_s}) = V^{c_s^-}\varphi^{c_s} + \mathcal{O}(h),\\ &E\varphi(x_{m_s}) = E\varphi^{c_s} + \mathcal{O}(h),\\ &-\frac{1}{2}\varepsilon^2\varphi_{xx}^{c_s^-} + V^{c_s^-}\varphi^{c_s} = E\varphi^{c_s}.\end{aligned}$$

Then we can write the modified approximation as [18]

$$\gamma_1^{m_s}\varphi^{m_s-1} + \gamma_2^{m_s}\varphi^{m_s} + \gamma_3^{m_s}\varphi^{m_s+1} + V^{m_s}\varphi^{m_s} = E\varphi^{m_s}. \tag{2.6}$$

This gives the local truncation error

$$\begin{aligned}T^{m_s} =&\gamma_1^{m_s}\varphi(x_{m_s-1}) + \gamma_2^{m_s}\varphi(x_{m_s}) + \gamma_3^{m_s}\varphi(x_{m_s+1}) + V(x_{m_s})\varphi(x_{m_s}) - E\varphi(x_{m_s})\\ =&\gamma_1^{m_s}\varphi(x_{m_s-1}) + \gamma_2^{m_s}\varphi(x_{m_s}) + \gamma_3^{m_s}\varphi(x_{m_s+1}) + V^{c_s^-}\varphi^{c_s} - E\varphi^{c_s} + \mathcal{O}(h)\\ =&\gamma_1^{m_s}\left(\varphi^{c_s} - (p_{s1}+1)h\varphi_x^{c_s} + \frac{1}{2}(p_{s1}+1)^2h^2\varphi_{xx}^{c_s^-}\right) + \gamma_2^{m_s}\left(\varphi^{c_s} - p_{s1}h\varphi_x^{c_s} + \frac{1}{2}p_{s1}^2h^2\varphi_{xx}^{c_s^-}\right)\\ &+\gamma_3^{m_s}\left(\varphi^{c_s} + p_{s2}h\varphi_x^{c_s} + \frac{1}{2}p_{s2}^2h^2\left(\varphi_{xx}^{c_s^-} + \frac{2[V]_{c_s}}{\varepsilon^2}\varphi^{c_s}\right)\right) + \frac{1}{2}\varepsilon^2\varphi_{xx}^{c_s^-} + \mathcal{O}(h)\\ =&\left(\gamma_1^{m_s} + \gamma_2^{m_s} + \gamma_3^{m_s}\left(1 + p_{s2}^2\tau^2[V]_{c_s}\right)\right)\varphi^{c_s} + \left(-(p_{s1}+1)\gamma_1^{m_s} - p_{s1}\gamma_2^{m_s} + p_{s2}\gamma_3^{m_s}\right)h\varphi_x^{c_s}\\ &+\frac{1}{2}\left((p_{s1}+1)^2\gamma_1^{m_s} + p_{s1}^2\gamma_2^{m_s} + p_{s2}^2\gamma_3^{m_s} + \frac{1}{\tau^2}\right)h^2\varphi_{xx}^{c_s^-} + \mathcal{O}(h).\end{aligned}$$

Therefore we have a linear system for the coefficients in (2.6)

$$\begin{cases}\gamma_1^{m_s} + \gamma_2^{m_s} + \gamma_3^{m_s}\left(1 + p_{s2}^2\tau^2[V]_{c_s}\right) = 0,\\ -(p_{s1}+1)\gamma_1^{m_s} - p_{s1}\gamma_2^{m_s} + p_{s2}\gamma_3^{m_s} = 0,\\ (p_{s1}+1)^2\gamma_1^{m_s} + p_{s1}^2\gamma_2^{m_s} + p_{s2}^2\gamma_3^{m_s} = -\dfrac{1}{\tau^2}.\end{cases} \tag{2.7}$$

By a similar process, we can modify the finite difference approximation at $n = m_s + 1$

$$\gamma_1^{m_s+1}\varphi^{m_s} + \gamma_2^{m_s+1}\varphi^{m_s+1} + \gamma_3^{m_s+1}\varphi^{m_s+2} + V^{m_s+1}\varphi^{m_s+1} = E\varphi^{m_s+1}, \tag{2.8}$$

in which the coefficients satisfy

$$\begin{cases}\gamma_1^{m_s+1}\left(1 - p_{s1}^2\tau^2[V]_{c_s}\right) + \gamma_2^{m_s+1} + \gamma_3^{m_s+1} = 0,\\ -p_{s1}\gamma_1^{m_s+1} + p_{s2}\gamma_2^{m_s+1} + (p_{s2}+1)\gamma_3^{m_s+1} = 0,\\ p_{s1}^2\gamma_1^{m_s+1} + p_{s2}^2\gamma_2^{m_s+1} + (p_{s2}+1)^2\gamma_3^{m_s+1} = -\dfrac{1}{\tau^2}.\end{cases} \tag{2.9}$$

We can simply compute the local truncation error

$$\begin{aligned}T^{m_s+1} =&\gamma_1^{m_s+1}\varphi(x_{m_s}) + \gamma_2^{m_s+1}\varphi(x_{m_s+1}) + \gamma_3^{m_s+1}\varphi(x_{m_s+2})\\ &+V(x_{m_s+1})\varphi(x_{m_s+1}) - E\varphi(x_{m_s+1})\\ =&\mathcal{O}(h).\end{aligned}$$

Remark 2.2. As discussed in [18], only four grid points (independent of h) are involved. Their $\mathcal{O}(h)$ local truncation errors are sufficient to ensure the numerical solution converges at least quadratically.

For the one dimensional eigenvalue problem of Schrödinger equation

$$-\frac{1}{2}\varepsilon^2\phi_{xx}+V\phi=E\phi, \tag{2.10}$$

with potential (2.2)–(2.3), we have the same jump conditions as (2.4). The numerical scheme is similarly given by (2.5)–(2.9).

At last, we consider the one dimensional dynamic Schrödinger equation

$$i\varepsilon\psi_t+\frac{1}{2}\varepsilon^2\psi_{xx}=V\psi, \tag{2.11}$$

with potential (2.2)–(2.3), here $\psi=\psi(t,x)$. The jump conditions are

$$\begin{cases} [V]_{c_1}=\Lambda, \quad [V]_{c_2}=-\Lambda, \\ [\psi]_{c_s}=0, \quad [\psi_x]_{c_s}=0, \quad [\psi_t]_{c_s}=0, \\ -\frac{1}{2}\varepsilon^2[\psi_{xx}]_{c_s}+[V]_{c_s}\psi^{c_s}=0. \end{cases}$$

The time grid is

$$t_l=lk, \quad l=0,1,\cdots,L,$$

where $k=T/L$. For $n\neq m_s,m_s+1$ the solution is smooth in the interval $[x_{n-1},x_{n+1}]$, and the Crank-Nicolson approximation can be used

$$\begin{aligned}\frac{\psi^{l+1,n}-\psi^{l,n}}{\omega}=&-\frac{1}{2\tau^2}\frac{1}{2}\Big((\psi^{l+1,n-1}-2\psi^{l+1,n}+\psi^{l+1,n+1})\\ &+(\psi^{l,n-1}-2\psi^{l,n}+\psi^{l,n+1})\Big)+\frac{V^n}{2}\left(\psi^{l+1,n}+\psi^{l,n}\right),\end{aligned}$$

with $\omega=k/(i\varepsilon)$. This gives a local truncation error

$$\begin{aligned}T^{l,n}=&\frac{i\varepsilon}{k}\Big(\psi(t_{l+1},x_n)-\psi(t_l,x_n)\Big)+\frac{\varepsilon^2}{4h^2}\Big(\psi(t_{l+1},x_{n-1})-2\psi(t_{l+1},x_n)+\psi(t_{l+1},x_{n+1})\Big)\\ &+\frac{\varepsilon^2}{4h^2}\Big(\psi(t_l,x_{n-1})-2\psi(t_l,x_n)+\psi(t_l,x_{n+1})\Big)-\frac{1}{2}V(x_n)\Big(\psi(t_{l+1},x_n)+\psi(t_l,x_n)\Big)\\ =&\mathcal{O}(h^2+k^2).\end{aligned}$$

For $n = m_s$ or $n = m_s + 1$, the modified approximations are

$$\begin{aligned}
\frac{\psi^{l+1,m_s} - \psi^{l,m_s}}{\omega} &= \frac{1}{2}\Big((\gamma_1^{m_s}\psi^{l+1,m_s-1} + \gamma_2^{m_s}\psi^{l+1,m_s} + \gamma_3^{m_s}\psi^{l+1,m_s+1}) \\
&\quad + (\gamma_1^{m_s}\psi^{l,m_s-1} + \gamma_2^{m_s}\psi^{l,m_s} + \gamma_3^{m_s}\psi^{l,m_s+1})\Big) + \frac{V^{m_s}}{2}\left(\psi^{l+1,m_s} + \psi^{l,m_s}\right), \\
\frac{\psi^{l+1,m_s+1} - \psi^{l,m_s+1}}{\omega} &= \frac{1}{2}\Big((\gamma_1^{m_s+1}\psi^{l+1,m_s} + \gamma_2^{m_s+1}\psi^{l+1,m_s+1} + \gamma_3^{m_s+1}\psi^{l+1,m_s+2}) \\
&\quad + (\gamma_1^{m_s+1}\psi^{l,m_s} + \gamma_2^{m_s+1}\psi^{l,m_s+1} + \gamma_3^{m_s+1}\psi^{l,m_s+2})\Big) \\
&\quad + \frac{V^{m_s+1}}{2}\left(\psi^{l+1,m_s+1} + \psi^{l,m_s+1}\right),
\end{aligned}$$

where γ_i^m are solutions of (2.7) and (2.9). Then the local truncation errors are

$$T^{l,m_s} = \mathcal{O}(h + k^2), \quad T^{l,m_s+1} = \mathcal{O}(h + k^2).$$

2.1. A special case for δ-potential

In this subsection, we consider the one dimensional stationary Schrödinger equation (2.1) with δ-potential

$$V_d(x) = \Lambda\delta(x - c_1).$$

Then the jump conditions are

$$[\varphi] = 0, \quad \frac{1}{2}\varepsilon^2\left[\varphi_x\right]_{c_1} = \Lambda\varphi^{c_1}, \quad [\varphi_{xx}] = 0,$$

from which we can derive linear systems for the coefficients in (2.6),

$$\begin{cases}
\gamma_1^{m_s} + \gamma_2^{m_s} + \gamma_3^{m_s}\left(1 + 2p_{s2}\tau\Lambda/\varepsilon\right) = 0, \\
-(p_{s1} + 1)\gamma_1^{m_s} - p_{s1}\gamma_2^{m_s} + p_{s2}\gamma_3^{m_s} = 0, \\
(p_{s1} + 1)^2\gamma_1^{m_s} + p_{s1}^2\gamma_2^{m_s} + p_{s2}^2\gamma_3^{m_s} = -\dfrac{1}{\tau^2},
\end{cases} \tag{2.12}$$

and in (2.8),

$$\begin{cases}
\gamma_1^{m_s+1}\left(1 + 2p_{s1}\tau\Lambda/\varepsilon\right) + \gamma_2^{m_s+1} + \gamma_3^{m_s+1} = 0, \\
-p_{s1}\gamma_1^{m_s+1} + p_{s2}\gamma_2^{m_s+1} + \left(p_{s2} + 1\right)\gamma_3^{m_s+1} = 0, \\
p_{s1}^2\gamma_1^{m_s+1} + p_{s2}^2\gamma_2^{m_s+1} + (p_{s2} + 1)^2\gamma_3^{m_s+1} = -\dfrac{1}{\tau^2}.
\end{cases} \tag{2.13}$$

These coefficients can be used analogously for the eigenvalue problem (2.10) and the dynamic problem (2.11).

3. Two dimensional Schrödinger equation

Now, we are turning to the two dimensional stationary Schrödinger equation

$$-\frac{1}{2}\varepsilon^2\left(\varphi_{xx}+\varphi_{yy}\right)+V\varphi=E\varphi, \tag{3.1}$$

on a computational domain $\Omega\subset\mathbb{R}^2$. The potential $V(x)$ is split into a smooth part $V_s(x,y)\in C^\infty(\Omega)$ and a discontinuous part $V_d(x,y)$:

$$V(x,y)=V_s(x)+V_d(x), \tag{3.2}$$

$$V_d(x,y)=\begin{cases}\Lambda, & (x,y)\in\Omega_d\subset\Omega,\\ 0, & \text{else.}\end{cases} \tag{3.3}$$

Assume Ω_d is a simply connected closed domain and $\Gamma_d=\partial\Omega_d$ is a smooth curve lying in Ω. Therefore, we can define a smooth indicate function $\mathscr{F}(x,y)$ such that

$$\begin{aligned}&\mathscr{F}(x,y)>0, && (x,y)\in\Omega_d\setminus\Gamma_d,\\ &\mathscr{F}(x,y)=0, && (x,y)\in\Gamma_d,\\ &\mathscr{F}(x,y)<0, && (x,y)\in\Omega\setminus\Omega_d.\end{aligned}$$

Remark 3.1. The discontinuous potential $V_d(x,y)$ can be considered in a general form. To concentrate on the key idea, we use (3.3) in this Section without any special instructions.

Let the computational domain be a square, say $[a_1,b_1]\times[a_2,b_2]$. We would like to compute the numerical solution of $\varphi(x,y)$ on a uniform grid

$$\begin{aligned}&x_n=nh+a_1, && n=0,1,\cdots,N,\\ &y_m=mh+a_2, && m=0,1,\cdots,M,\end{aligned}$$

where

$$h=\frac{b_1-a_1}{N}=\frac{b_2-a_2}{M}.$$

For a regular grid point (x_n,y_m),

$$\begin{aligned}&\mathscr{F}(x_n,y_m)\mathscr{F}(x_{n'},y_{m'})>0, \quad \forall(x_{n'},y_{m'})\in S^{n,m},\\ &S^{n,m}=\Big\{(x_n,y_m),\,(x_{n-1},y_m),\,(x_{n+1},y_m),\,(x_n,y_{m-1}),\,(x_n,y_{m+1})\Big\},\end{aligned}$$

we can use the standard five points approximation

$$-\frac{\varepsilon^2}{2h^2}\left(\varphi^{n-1,m}+\varphi^{n,m-1}-4\varphi^{n,m}+\varphi^{n+1,m}+\varphi^{n,m+1}\right)+V^{n,m}\varphi^{n,m}=E\varphi^{n,m},$$

with a local truncation error

$$T^{n,m}=-\frac{\varepsilon^2}{2h^2}\left(\varphi^{n-1,m}+\varphi^{n,m-1}-4\varphi^{n,m}+\varphi^{n+1,m}+\varphi^{n,m+1}\right)+\left(V^{n,m}-E\right)\varphi^{n,m}=\mathscr{O}(h^2).$$

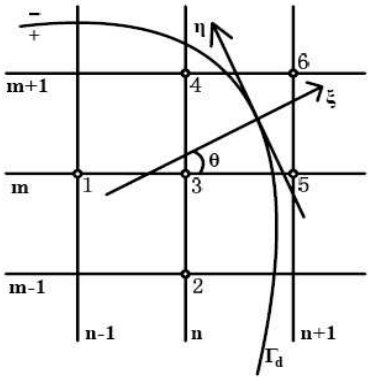

Figure 1: Interface Γ_d in a two dimensional domain and the local coordinate (ξ, η).

For irregular points, the standard five points are on the different sides of the interface, which means that the standard approximation may not work. To design the new finite difference scheme, we firstly look for $(x_n^0, y_m^0) \in \Gamma_d$, who is closest to (x_n, y_m). Taking (x_n^0, y_m^0) as the original point, we construct a local coordinate (see Fig. 1) with the following transformation

$$\begin{pmatrix} x \\ y \end{pmatrix} = \begin{pmatrix} \cos\theta & -\sin\theta \\ \sin\theta & \cos\theta \end{pmatrix} \begin{pmatrix} \xi \\ \eta \end{pmatrix} + \begin{pmatrix} x_n^0 \\ y_m^0 \end{pmatrix},$$

where ξ and η are in the normal and tangential directions of the interface, and θ is the rotation angle. The stationary Schrödinger equation (3.1) can be rewritten in the local coordinate system as

$$-\frac{1}{2}\varepsilon^2 \left(\varphi_{\xi\xi} + \varphi_{\eta\eta}\right) + V\varphi = E\varphi.$$

Then we can give the jump conditions at (x_n^0, y_m^0):

$$\begin{cases} [V] = \Lambda, \quad [\varphi] = \left[\varphi_\xi\right] = \left[\varphi_\eta\right] = 0, \\ \left[\varphi_{\xi\eta}\right] = \left[\varphi_{\eta\eta}\right] = 0, \quad \left[\varphi_{\xi\xi}\right] = \dfrac{2}{\varepsilon^2}[V]\,\varphi. \end{cases} \tag{3.4}$$

Here $[\cdot]$ represents the jump in a quantity at the point (x_n^0, y_m^0)

$$[\varphi] = \varphi^+ - \varphi^-.$$

We use superscripts $+$ or $-$ to denote the limiting values of a function from one side (in Ω_d) or the other (in $\Omega \setminus \Omega_d$). It is easy to see there are six constraints, thus we need an additional point (x_n^*, y_m^*) to close the system. We choose

$$(x_n^*, y_m^*) \in \widehat{S}^{n,m} = \left\{(x_{n-1}, y_{m-1}),\ (x_{n-1}, y_{m+1}),\ (x_{n+1}, y_{m-1}),\ (x_{n+1}, y_{m+1})\right\}$$

to be the closest point to (x_n^0, y_m^0). Then we can define the following sets

$$S_*^{n,m} = S^{n,m} \cup \{(x_n^*, y_m^*)\},$$
$$S_+^{n,m} = S_*^{n,m} \cap \Omega_d, \qquad S_-^{n,m} = S_*^{n,m} \cap (\Omega \setminus \Omega_d).$$

We write the Taylor expansion for $(x, y) \in S_{n,m}^+$

$$\varphi(\xi, \eta) = \varphi^+ + \varphi_\xi^+ \xi + \varphi_\eta^+ \eta + \frac{1}{2}\varphi_{\xi\xi}^+ \xi^2 + \varphi_{\xi\eta}^+ \xi\eta + \frac{1}{2}\varphi_{\eta\eta}^+ \eta^2 + \mathcal{O}(h^3),$$

and for $(x, y) \in S_{n,m}^-$

$$\varphi(\xi, \eta) = \varphi^- + \varphi_\xi^- \xi + \varphi_\eta^- \eta + \frac{1}{2}\varphi_{\xi\xi}^- \xi^2 + \varphi_{\xi\eta}^- \xi\eta + \frac{1}{2}\varphi_{\eta\eta}^- \eta^2 + \mathcal{O}(h^3).$$

Here $\varphi, \varphi_\xi^\pm, \varphi_\eta^\pm, \varphi_{\xi\xi}^\pm, \varphi_{\xi\eta}^\pm$ and $\varphi_{\eta\eta}^\pm$ denote the corresponding limiting values of φ at point (x_n^0, y_m^0). For $(x_n, y_m) \in S_{n,m}^+$, we have

$$V(x_n, y_m)\varphi(x_n, y_m) = V^+\varphi^+ + \mathcal{O}(h),$$
$$E\varphi(x_n, y_m) = E\varphi^+ + \mathcal{O}(h),$$
$$-\frac{1}{2}\varepsilon^2\left(\varphi_{\xi\xi}^+ + \varphi_{\eta\eta}^+\right) + V^+\varphi^+ = E\varphi^+.$$

We write the modified approximation as

$$\sum_{s \in S_+^{n,m}} \gamma_s^{n,m}\varphi_s^{n,m} + \sum_{s \in S_-^{n,m}} \gamma_s^{n,m}\varphi_s^{n,m} + V^{n,m}\varphi^{n,m} = E\varphi^{n,m}. \tag{3.5}$$

To make the equation clear, the indexes (n, m) are dropped

$$\sum_{s \in S_+} \gamma_s\varphi_s + \sum_{s \in S_-} \gamma_s\varphi_s + V\varphi = E\varphi.$$

This gives the local truncation error

$$\begin{aligned}
T &= \sum_{s \in S_+} \gamma_s\varphi(x_s, y_s) + \sum_{s \in S_-} \gamma_s\varphi(x_s, y_s) + (V(x_n, y_m) - E)\varphi(x_n, y_m) \\
&= \sum_{s \in S_+} \gamma_s\left(\varphi^+ + \varphi_\xi^+\xi_s + \varphi_\eta^+\eta_s + \frac{1}{2}\varphi_{\xi\xi}^+\xi_s^2 + \varphi_{\xi\eta}^+\xi_s\eta_s + \frac{1}{2}\varphi_{\eta\eta}^+\eta_s^2\right) + \left(V^+ - E\right)\varphi^+ \\
&\quad + \sum_{s \in S_-} \gamma_s\left(\varphi^- + \varphi_\xi^-\xi_s + \varphi_\eta^-\eta_s + \frac{1}{2}\varphi_{\xi\xi}^-\xi_s^2 + \varphi_{\xi\eta}^-\xi_s\eta_s + \frac{1}{2}\varphi_{\eta\eta}^-\eta_s^2\right) + \mathcal{O}(h) \\
&= \sum_{s \in S_+} \gamma_s\left(\varphi^+ + \varphi_\xi^+\xi_s + \varphi_\eta^+\eta_s + \frac{1}{2}\varphi_{\xi\xi}^+\xi_s^2 + \varphi_{\xi\eta}^+\xi_s\eta_s + \frac{1}{2}\varphi_{\eta\eta}^+\eta_s^2\right) \\
&\quad + \sum_{s \in S_-} \gamma_s\left(\varphi^+ + \varphi_\xi^+\xi_s + \varphi_\eta^+\eta_s + \frac{1}{2}\left(\varphi_{\xi\xi}^+ - \frac{2}{\varepsilon^2}[V]\varphi^+\right)\xi_s^2 + \varphi_{\xi\eta}^+\xi_s\eta_s + \frac{1}{2}\varphi_{\eta\eta}^+\eta_s^2\right) \\
&\quad + \frac{1}{2}\varepsilon^2\left(\varphi_{\xi\xi}^+ + \varphi_{\eta\eta}^+\right) + \mathcal{O}(h).
\end{aligned}$$

Therefore we have a linear system for the coefficients

$$\begin{cases} \sum_{s\in S_*}\gamma_s - \frac{[V]}{\varepsilon^2}\sum_{s\in S_-}\xi_s^2\gamma_s = 0, & \sum_{s\in S_*}\xi_s^2\gamma_s = -\varepsilon^2, \\ \sum_{s\in S_*}\xi_s\gamma_s = 0, & \sum_{s\in S_*}\xi_s\eta_s\gamma_s = 0, \\ \sum_{s\in S_*}\gamma_s\eta_s = 0, & \sum_{s\in S_*}\eta_s^2\gamma_s = -\varepsilon^2. \end{cases} \tag{3.6}$$

For $(x_n, y_m) \in S_-^{n,m}$, we have

$$\begin{aligned} &V(x_n, y_m)\varphi(x_n, y_m) = V^-\varphi^- + \mathcal{O}(h), \\ &E\varphi(x_n, y_m) = E\varphi^- + \mathcal{O}(h), \\ &-\frac{1}{2}\varepsilon^2\left(\varphi^-_{\xi\xi} + \varphi^-_{\eta\eta}\right) + V^-\varphi^- = E\varphi^-. \end{aligned}$$

Then the coefficients for the modified approximation (3.5) satisfy the following linear system

$$\begin{cases} \sum_{s\in S_*}\gamma_s + \frac{[V]}{\varepsilon^2}\sum_{s\in S_+}\xi_s^2\gamma_s = 0, & \sum_{s\in S_*}\xi_s^2\gamma_s = -\varepsilon^2, \\ \sum_{s\in S_*}\xi_s\gamma_s = 0, & \sum_{s\in S_*}\xi_s\eta_s\gamma_s = 0, \\ \sum_{s\in S_*}\eta_s\gamma_s = 0, & \sum_{s\in S_*}\eta_s^2\gamma_s = -\varepsilon^2, \end{cases} \tag{3.7}$$

from which, we can compute the local truncation error

$$\begin{aligned} T =& \sum_{s\in S_+}\gamma_s\varphi(x_s, y_s) + \sum_{s\in S_-}\gamma_s\varphi(x_s, y_s) + \big(V(x_n, y_m) - E\big)\varphi(x_n, y_m) \\ =& \mathcal{O}(h). \end{aligned}$$

Remark 3.2. As discussed in [18], the irregular points, which are adjacent to the curve Γ_d, form a lower-dimensional set. Their $\mathcal{O}(h)$ local truncation errors are sufficient to ensure the numerical solution converges at least quadratically, just as in one dimension.

For the two dimensional eigenvalue problem of Schrödinger equation

$$-\frac{1}{2}\varepsilon^2\left(\phi_{xx} + \phi_{yy}\right) + V\phi = E\phi, \tag{3.8}$$

and dynamic Schrödinger equation

$$i\varepsilon\psi_t + \frac{1}{2}\varepsilon^2\left(\psi_{xx} + \psi_{yy}\right) = V\psi, \tag{3.9}$$

with potential (3.2)–(3.3), the numerical schemes can be similarly derived. We omit the details and leave them to the readers.

4. Numerical examples

In this section, we will present a few examples to test the order of accuracy for the numerical scheme.

Example 1. We consider the one dimensional Schrödinger equation with the following parameters

$$a=-1,\quad b=1,\quad c_1=-\frac{\sqrt{2}}{4},\quad c_2=\frac{\sqrt{2}}{4},$$
$$\Lambda=1,\quad V_s(x)=0.1\sin\pi x.$$

(i) For the stationary Schrödinger equation (2.1) with the following transparent boundary condition

$$\begin{aligned}&\varepsilon\varphi_x(a)+i\sqrt{2(E-V(a))}\varphi(a)=2i\sqrt{2(E-V(a))},\\&\varepsilon\varphi_x(b)-i\sqrt{2(E-V(b))}\varphi(b)=0,\end{aligned}\tag{4.1}$$

where $\varepsilon=0.1$, we output the l^∞ errors of wave functions for different energies E and mesh sizes h in Table 1. In Fig. 2, the wave amplitudes $|\varphi(x)|$ are plotted versus different energies E.

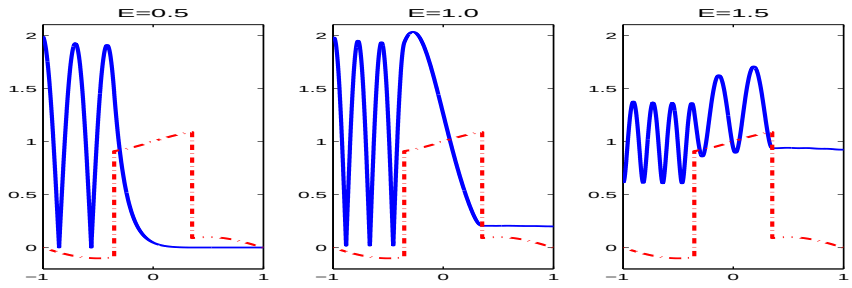

Figure 2: Example 1-1, the wave amplitude $|\varphi(x)|$ (blue solid lines) for different energies E. The red dash-dot lines are the potential profile.

(ii) For the eigenvalue problem of Schrödinger equation (2.10) with the periodic boundary condition (pbc)

$$\phi(x+(b-a))=\phi(x),$$

or the reflection boundary condition (rbc)

$$\phi(a)=\phi(b)=0,$$

where $\varepsilon=0.1$, we output the l^∞ errors of the first ten eigenvectors for different mesh size h in Table 2. In Fig. 3, the wave functions of the first ten eigenvectors $\phi(x)$ are plotted. Since the eigenvalues E are corresponding to the total energies $E_T=|p|^2/2+V$, they can be negative when the potential energy $V(x)$ is negative.

Table 1: Example 1-1, the l^∞ errors of $\varphi(x)$ for different energies E and mesh sizes h. The numerical solutions are computed by both the standard finite difference approximation (SFA) and the immersed interface method (IIM).

h	$\frac{1}{200}$	$\frac{1}{400}$	$\frac{1}{800}$	$\frac{1}{1600}$
$E=0.5$ (SFA)	1.09×10^{-1}	6.19×10^{-2}	1.53×10^{-2}	7.59×10^{-3}
ratio	$---$	1.76	4.05	2.02
$E=0.5$ (IIM)	1.44×10^{-3}	3.86×10^{-4}	7.57×10^{-5}	1.76×10^{-5}
ratio	$---$	3.73	5.10	4.30
$E=1.0$ (SFA)	1.83×10^{-1}	6.60×10^{-2}	3.14×10^{-2}	1.15×10^{-2}
ratio	$---$	2.77	2.10	2.73
$E=1.0$ (IIM)	4.73×10^{-3}	1.18×10^{-3}	2.88×10^{-4}	5.73×10^{-5}
ratio	$---$	4.01	4.10	5.03
$E=1.5$ (SFA)	1.13×10^{-1}	5.51×10^{-2}	2.13×10^{-2}	8.88×10^{-3}
ratio	$---$	2.05	2.59	2.40
$E=1.5$ (IIM)	8.72×10^{-3}	2.17×10^{-3}	5.12×10^{-4}	1.03×10^{-4}
ratio	$---$	4.02	4.24	4.97

Table 2: Example 1-2, the l^∞ errors of $\phi(x)$ for different mesh sizes h.

h	$\frac{1}{200}$	$\frac{1}{400}$	$\frac{1}{800}$	$\frac{1}{1600}$
pbc (SFA)	5.44×10^{-2}	2.20×10^{-2}	1.03×10^{-2}	4.03×10^{-3}
ratio	$---$	2.47	2.14	2.56
pbc (IIM)	1.92×10^{-3}	4.82×10^{-4}	1.09×10^{-4}	2.26×10^{-5}
ratio	$---$	3.98	4.42	4.82
rbc (SFA)	6.76×10^{-2}	2.92×10^{-2}	1.25×10^{-2}	4.83×10^{-3}
ratio	$---$	2.32	2.34	2.59
rbc (IIM)	1.97×10^{-3}	4.95×10^{-4}	1.12×10^{-4}	2.32×10^{-5}
ratio	$---$	3.98	4.42	4.83

(iii) For the dynamic Schrödinger equation (2.11) with the periodic boundary condition (pbc)

$$\psi(t,x+(b-a))=\psi(t,x),$$

or the reflection boundary condition (rbc)

$$\psi(t,a)=\psi(t,b)=0,$$

with $\varepsilon=0.02$, $T_f=0.54$, and the initial data

$$\psi_0(x)=e^{-400(x+0.6)^2}e^{\frac{i(x+1)}{\varepsilon}},$$

we output the l^∞ errors of wave functions for different mesh sizes h at time $t=T_f$ in Table 3. In Fig. 4, the wave amplitudes $|\psi(t,x)|$ are plotted. To investigate the stability of the immersed interface method for the dynamic problem, we output the l^∞ errors of the

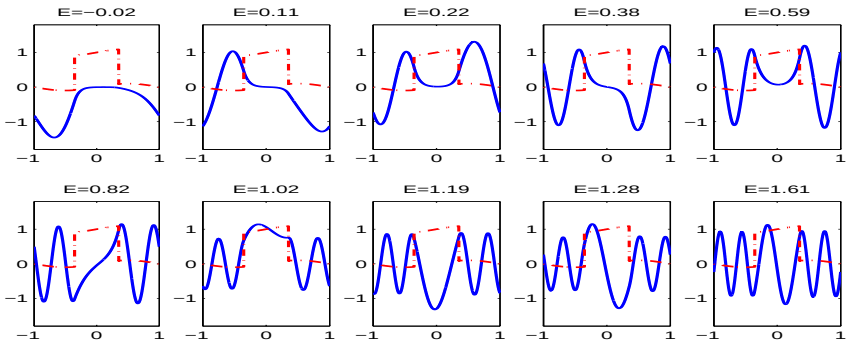

(a) Periodic boundary condition

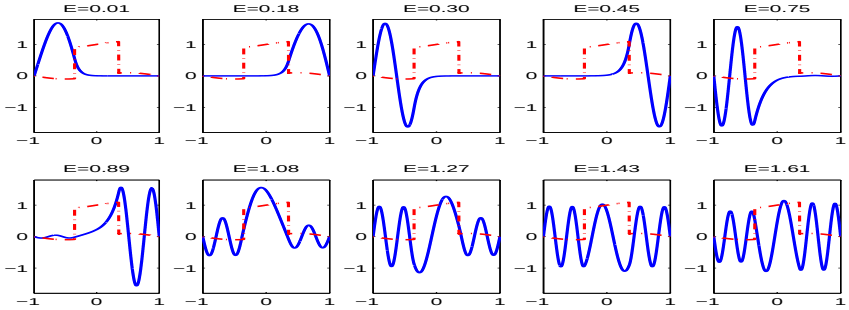

(b) Reflection boundary condition

Figure 3: Example 1-2, the wave functions of the first ten eigenvectors $\phi(x)$.

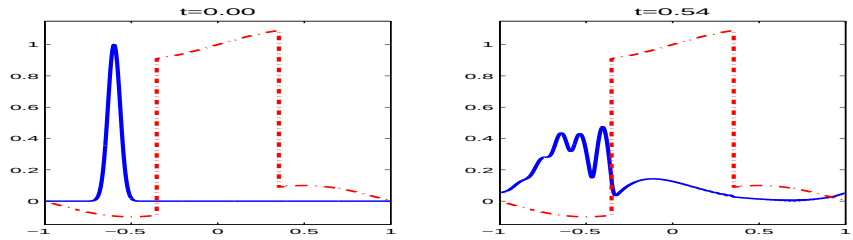

(a) Periodic boundary condition.

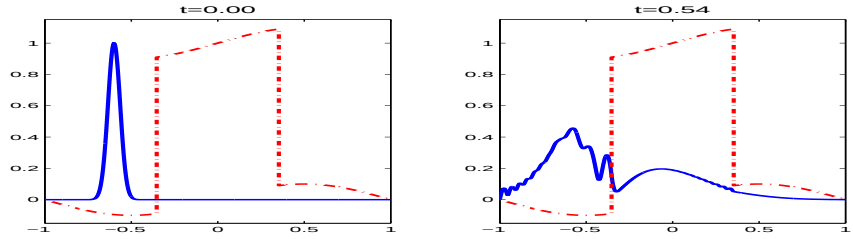

(b) Reflection boundary condition.

Figure 4: Example 1-3, the initial and final wave amplitude $|\psi(t,x)|$.

Table 3: Example 1-3, the l^∞ errors of $\psi(t,x)$ for different mesh sizes h and time steps k.

(h,k)	$\left(\frac{1}{1000},\frac{1}{1000}\right)$	$\left(\frac{1}{2000},\frac{1}{2000}\right)$	$\left(\frac{1}{4000},\frac{1}{4000}\right)$	$\left(\frac{1}{8000},\frac{1}{8000}\right)$
pbc (SFA)	6.32×10^{-2}	2.80×10^{-2}	1.18×10^{-2}	4.76×10^{-3}
ratio	$---$	2.26	2.37	2.48
pbc (IIM)	9.23×10^{-4}	2.34×10^{-4}	5.58×10^{-5}	1.11×10^{-5}
ratio	$---$	3.94	4.19	5.03
rbc (SFA)	6.20×10^{-2}	2.80×10^{-2}	1.20×10^{-2}	4.92×10^{-3}
ratio	$---$	2.21	2.33	2.44
rbc (IIM)	1.52×10^{-3}	3.90×10^{-4}	9.15×10^{-5}	1.79×10^{-5}
ratio	$---$	3.90	4.26	5.11

Table 4: Example 1-3, the l^∞ errors of $\psi(t,x)$ for different final times $t=T_f$.

(h,k)	$\left(\frac{1}{1000},\frac{1}{1000}\right)$	$\left(\frac{1}{2000},\frac{1}{2000}\right)$	$\left(\frac{1}{4000},\frac{1}{4000}\right)$	$\left(\frac{1}{8000},\frac{1}{8000}\right)$
pbc ($T_f=0.54$)	9.23×10^{-4}	2.34×10^{-4}	5.58×10^{-5}	1.11×10^{-5}
ratio	$---$	3.94	4.19	5.03
pbc ($T_f=1.08$)	6.10×10^{-3}	1.52×10^{-3}	3.61×10^{-4}	7.22×10^{-5}
ratio	$---$	4.01	4.21	5.00
pbc ($T_f=2.16$)	1.20×10^{-2}	3.08×10^{-3}	7.36×10^{-4}	1.47×10^{-4}
ratio	$---$	3.90	4.18	5.01
rbc ($T_f=0.54$)	1.52×10^{-3}	3.90×10^{-4}	9.15×10^{-5}	1.79×10^{-5}
ratio	$---$	3.90	4.26	5.11
rbc ($T_f=1.08$)	8.56×10^{-3}	2.12×10^{-3}	5.03×10^{-4}	1.01×10^{-4}
ratio	$---$	4.04	4.21	4.98
rbc ($T_f=2.16$)	2.34×10^{-2}	6.13×10^{-3}	1.47×10^{-3}	2.94×10^{-4}
ratio	$---$	3.82	4.17	5.00

wave functions for different final time T_f in Table 4. We can see the convergence rate is almost independent of time.

From all these data, we can observe that the numerical solutions of the immersed interface method converges at least in second order.

Remark 4.1. In this example, together with later examples, the reference Schrödinger solutions are computed by using the standard finite difference approximation. And we use the discrete discontinuous function and delta function technical given in [32, 35]. Since the standard finite difference approximation converges in about first order, we can believe that the reference solutions are accurate enough if we take a very fine mesh size and a very small time step, e.g.,

- For the stationary problem, we take $h=10^{-6}$.
- For the eigenvalue problem, we take $h=10^{-6}$.
- For the time dependent problem, we take $h=k=10^{-7}$.

Example 2. We consider the one dimensional Schrödinger equation on the computational domain $[-1,1]$ with δ-potential

$$V(x)=2\left(x-\frac{\sqrt{3}}{20}\right)^2-1+\frac{1}{10}\delta\left(x-\frac{\sqrt{3}}{20}\right).$$

(i) For the stationary Schrödinger equation (2.1) with the transparent boundary condition (4.1), with $\varepsilon=0.1$, we output the l^∞ errors of wave functions for different mesh sizes h in Table 5. In Fig. 5, the real and imaginary parts of wave function $\varphi(x)$ are plotted.

(ii) For the eigenvalue problem of Schrödinger equation (2.10) with the reflection boundary condition, with $\varepsilon=0.1$, we output the l^∞ errors of the first six eigenvectors for different mesh sizes h in Table 6. In Fig. 6, the wave functions of the first six eigenvectors $\phi(x)$ are plotted.

(iii) For the dynamic Schrödinger equation (2.11) with the periodic boundary condition, $\varepsilon=0.01$, $T_f=0.54$, and the initial data

$$\psi_0(x)=e^{-400(x+0.4)^2}e^{2i(x+1)/\varepsilon},$$

we output the l^∞ errors of the wave functions for different mesh sizes h at time $t=T_f$ in Table 7. In Fig. 7, the wave amplitudes $|\psi(t,x)|$ are plotted at time $t=0$, 0.23, 0.27, and 0.54. From which, we can draw the same conclusion as in Example 1.

Table 5: Example 2-1, the l^∞ errors of $\varphi(x)$ for different mesh sizes h.

h	$\frac{1}{200}$	$\frac{1}{400}$	$\frac{1}{800}$	$\frac{1}{1600}$
$E=1.5$ (SFA)	2.31×10^{-2}	1.27×10^{-2}	7.30×10^{-3}	4.10×10^{-3}
ratio	$---$	1.82	1.74	1.78
$E=1.5$ (IIM)	9.33×10^{-3}	2.31×10^{-3}	5.47×10^{-4}	1.11×10^{-4}
ratio	$---$	4.04	4.22	4.93

Table 6: Example 2-2, the l^∞ errors of $\phi(x)$ for different mesh sizes h.

h	$\frac{1}{200}$	$\frac{1}{400}$	$\frac{1}{800}$	$\frac{1}{1600}$
rbc (SFA)	4.54×10^{-2}	2.41×10^{-2}	1.24×10^{-2}	6.31×10^{-3}
ratio	$---$	1.88	1.94	1.97
rbc (IIM)	2.00×10^{-3}	5.00×10^{-4}	1.18×10^{-4}	2.45×10^{-5}
ratio	$---$	4.00	4.24	4.82

Table 7: Example 2-3, the l^∞ errors of $\psi(t,x)$ for different mesh sizes h and time steps k.

(h,k)	$\left(\frac{1}{1000},\frac{1}{1000}\right)$	$\left(\frac{1}{2000},\frac{1}{2000}\right)$	$\left(\frac{1}{4000},\frac{1}{4000}\right)$	$\left(\frac{1}{8000},\frac{1}{8000}\right)$
pbc (SFA)	8.60×10^{-2}	6.61×10^{-2}	4.37×10^{-2}	2.57×10^{-2}
ratio	$---$	1.30	1.51	1.70
pbc (IIM)	4.65×10^{-2}	1.11×10^{-2}	2.61×10^{-3}	5.21×10^{-4}
ratio	$---$	4.19	4.25	5.01

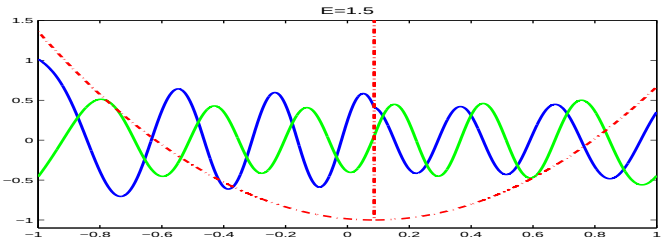

Figure 5: Example 2-1, the real part (blue solid line) and imaginary part (green solid line) of wave function $\varphi(x)$ for energy $E = 1.5$. The red dash-dot line is the potential profile.

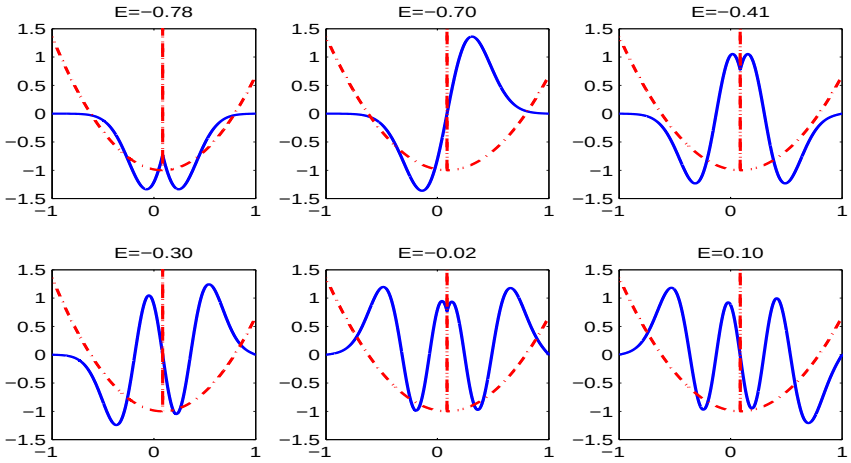

Figure 6: Example 2-2, the wave functions of the first six eigenvectors $\phi(x)$.

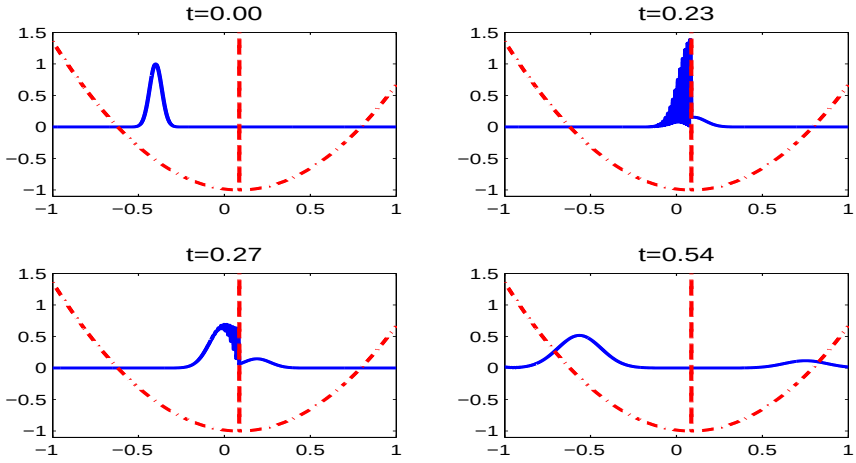

Figure 7: Example 2-3, the wave amplitude $|\psi(t,x)|$ at different time.

Example 3. We consider the two dimensional Schrödinger equation on the computational domain $\Omega=[-0.5,1]\times[-0.5,0.5]$ with potential

$$V(x,y)=\begin{cases}0.3, & (x-0.5)^2+y^2<0.093,\\ 0, & \text{else.}\end{cases}$$

(i) Consider the stationary Schrödinger equation (3.1) with the following boundary condition

$$\begin{aligned}&\varphi(x,\pm0.5)=0,\\ &\varepsilon\partial_x\varphi(-0.5,y)=\sum_{E>E_k} i\sqrt{2(E-E_k)}(2a_k-\varphi_k^l)\chi_k(y)+\sum_{E\le E_k}\sqrt{2(E_k-E)}\varphi_k^l\chi_k(y),\\ &\varepsilon\partial_x\varphi(1,y)=\sum_{E>E_k} i\sqrt{2(E-E_k)}\varphi_k^r\chi_k(y)-\sum_{E\le E_k}\sqrt{2(E_k-E)}\varphi_k^r\chi_k(y),\end{aligned}$$

where $(E_k,\chi_k(y))$ are solutions of the eigenvalue problem

$$\begin{cases}-\dfrac{1}{2}\varepsilon^2\partial_{yy}\chi(y)=E\chi(y),\\ \chi(\pm0.5)=0,\ \langle\chi(y),\chi(y)\rangle=1,\end{cases}\tag{4.2}$$

and

$$\begin{aligned}&\varphi(-0.5,y)=\sum_{k=1}^{\infty}\varphi_k^l\chi_k(y)\approx\sum_{k=1}^{K}\varphi_k^l\chi_k(y), && \text{with } \varphi_k^l=\langle\varphi(-0.5,y),\chi_k(y)\rangle,\\ &\varphi(1,y)=\sum_{k=1}^{\infty}\varphi_k^r\chi_k(y)\approx\sum_{k=1}^{K}\varphi_k^r\chi_k(y), && \text{with } \varphi_k^r=\langle\varphi(1,y),\chi_k(y)\rangle.\end{aligned}$$

The re-scaled Planck constant is $\varepsilon=0.1$. In Table 8, we present the first six eigenvalues of (4.2). From which we can believe that $K=6$ is accurate enough for the boundary condition when $E\le0.7$. The coefficients of incoming waves a_k are given by

$$a_k=\begin{cases}1, & k=1,2,\\ 0, & \text{else.}\end{cases}$$

We output the l^∞ errors of the wave amplitude for different energies E and mesh sizes h in Table 9. In Fig. 8, the wave amplitudes $|\varphi(x,y)|$ are plotted versus different energies E.

Table 8: Example 3-1, the first six eigenvalues of (4.2).

k	1	2	3	4	5	6
E_k	0.049	0.197	0.444	0.790	1.234	1.777

Table 9: Example 3-1, the l^∞ errors of $|\varphi(x,y)|$ for different energies E and mesh sizes h. The numerical solutions are computed by the immersed interface method.

h	$\frac{1}{40}$	$\frac{1}{80}$	$\frac{1}{160}$
$E=0.2$	3.88×10^{-2}	9.04×10^{-3}	1.79×10^{-3}
ratio	$---$	4.29	5.05
$E=0.4$	3.42×10^{-2}	8.29×10^{-3}	1.69×10^{-3}
ratio	$---$	4.13	4.91
$E=0.6$	5.23×10^{-2}	1.26×10^{-2}	2.53×10^{-3}
ratio	$---$	4.15	4.98

(ii) For the eigenvalue problem of Schrödinger equation (3.8) with the following boundary condition,

$$\phi(x,\pm0.5)=0,$$
$$\phi(x+1.5,y)=\phi(x,y),$$

where $\varepsilon=0.1$, we output the l^∞ errors of the first six eigenvalues and eigenvectors for different mesh sizes h in Table 10. In Fig. 9, the wave amplitudes of the first six eigenvectors $|\phi(x,y)|$ are plotted.

Table 10: Example 3-2, the l^∞ errors of E and $|\phi(x,y)|$ for different mesh sizes h. The numerical solutions are computed by the immersed interface method.

h	$\frac{1}{40}$	$\frac{1}{80}$	$\frac{1}{160}$
E	5.45×10^{-4}	1.28×10^{-4}	2.57×10^{-5}
ratio	$---$	4.26	4.98
$\lvert\phi(x,y)\rvert$	6.70×10^{-2}	1.65×10^{-2}	4.02×10^{-3}
ratio	$---$	4.06	4.10

(iii) For the dynamic Schrödinger equation (3.9) with the following boundary condition,

$$\psi(t,x,\pm0.5)=0,$$
$$\psi(t,x+1.5,y)=\psi(x,y),$$

$\varepsilon=0.05$, $T_f=0.6$, and the initial data

$$\psi_0(x,y)=e^{-40\left((x+0.05)^2+y^2\right)}e^{\frac{1.2i(x+1)}{\varepsilon}},$$

we output the l^∞ errors of the wave amplitude for different mesh sizes h at time $t=T_f$ in Table 11. In Fig. 10, the wave amplitudes $|\psi(t,x,y)|$ are plotted at time $t=0.15$, 0.3, 0.45, and 0.6. From which, we can draw the same conclusion as in Example 1.

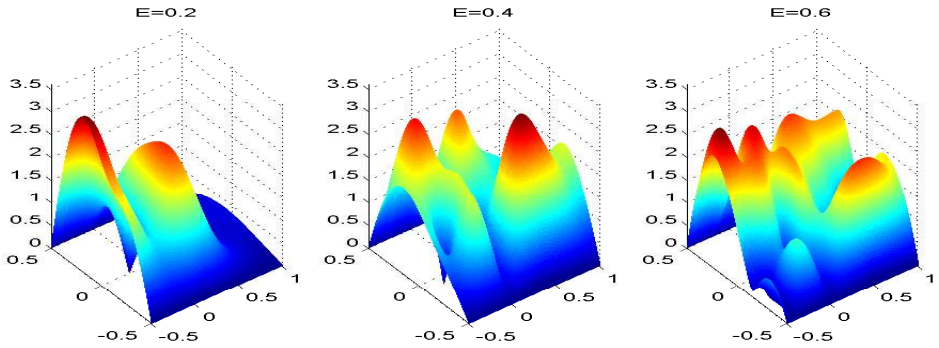

Figure 8: Example 3-1, the wave amplitude $|\varphi(x,y)|$ for different energies E.

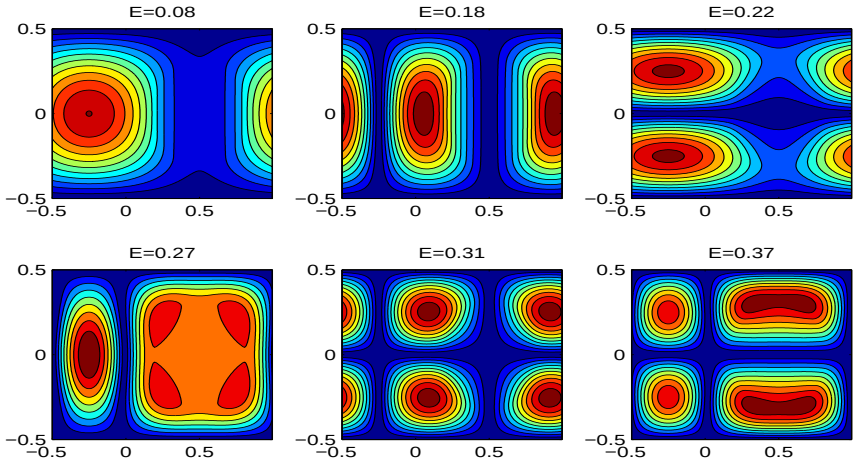

Figure 9: Example 3-2, the wave amplitude of the first six eigenvectors $|\phi(x,y)|$.

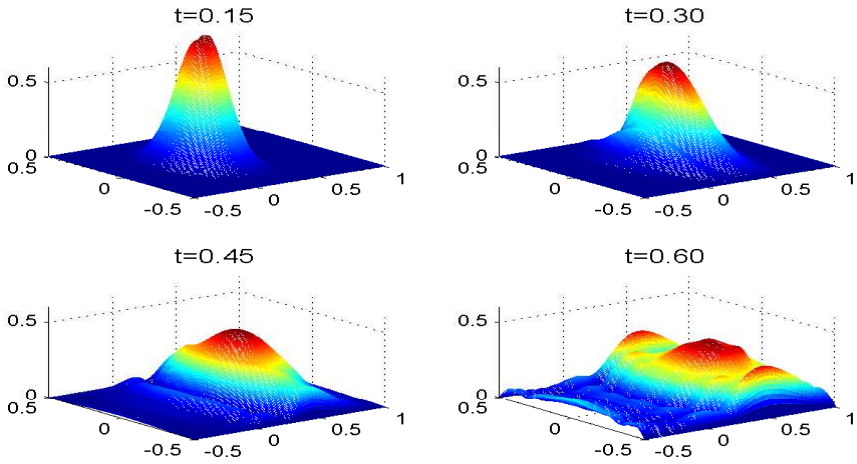

Figure 10: Example 3-3, the wave amplitude of $|\psi(t,x,y)|$.

Table 11: Example 3-3, the l^∞ errors of $|\psi(t,x,y)|$ for different mesh sizes h and time steps k. The numerical solutions are computed by the immersed interface method.

(h,k)	$\left(\frac{1}{40},\frac{1}{160}\right)$	$\left(\frac{1}{80},\frac{1}{160}\right)$	$\left(\frac{1}{160},\frac{1}{160}\right)$
$\|\psi(t,x,y)\|$	1.19×10^{-1}	2.90×10^{-2}	6.79×10^{-3}
ratio	$---$	4.10	4.27

5. Conclusion

Since the discontinuous potential would effect the continuity of wave function's derivatives, standard numerical methods for the Schrödinger equation with discontinuous potential give low accuracy. Since the Schrödinger equation with discontinuous potential is a basic model in many practical applications, a high order numerical method is required. For this reason, we modify the famous immersed interface method to give a second order scheme for this problem.

The issue of computing dynamic Schrödinger equation with discontinuous potential in the semiclassical regime is another interesting topic. It will be studied in a forthcoming paper [39]. The other interesting problem is how to design a high accurate, mass and energy conservation numerical scheme based on the immersed interface method for the dynamic Schrödinger equation with discontinuous potential. This topic is still under investigation.

Acknowledgments During this research, the author benefited from a Post Doc position supported by the Conseil regional Midi Pyrénées (http://www.midipyrenees.fr/) entitled "Méthodes Numériques Multi-échelles pour le transport quantique" and by the ANR Project No. BLAN07-2 212988 entitled "QUATRAIN"). He acknowledges support from NSFC Project 11071139 and NSFC Project 10971115. The author would also thank the anonymous reviewers for their great efforts and valuable comments in improving the quality of the manuscript.

References

[1] N. Ben Abdallah, *On a multidimensional Schrödinger-Poisson scattering model for semiconductors*, Joural of Mathematical Physics, 41(2000), no. 7, 4241-4261.

[2] N. Ben Abdallah, P. Degond and P.A. Markowich, *On a one-dimensional Schrödinger-Poisson scattering model*, Zeitschrift für Angewandte Mathematik und Physik., 48(1997), 135-155.

[3] N. Ben Abdallah, C. Negulescu, M. Mouis and E. Polizzi, *Simulation Schemes in 2D Nanoscale MOSFETs: A WKB Based Method*, Journal of Computational Electronics, 3(2004), 397-400.

[4] N. Ben Abdallah and O. Pinaud, *Multiscale simulation of transport in an open quantum system: Resonances and WKB interpolation*, Journal of Computational Physics, 213(2006), no. 1, 288-310.

[5] N. Ben Abdallah and H. Wu, *A generalized stationary algorithm for resonant tunneling: multi-mode approximation and high dimension*, Communications in Computational Physics, 10(2011), no. 4, 882-898.

[6] L. ADAMS AND Z.L. LI, *The immersed interface/multigrid methods for interface problems*, SIAM Journal on Scientific Computing, 24(2002), no. 2, 463-479.
[7] W.Z. BAO, S. JIN AND P.A. MARKOWICH, *On time-splitting spectral approximations for the Schrödinger equation in the semiclassical regime*, Journal of Computational Physics, 175(2002), 487-524.
[8] W.Z. BAO, S. JIN AND P.A. MARKOWICH, *Numerical studies of time-splitting spectral discretizations of nonlinear Schrödinger equations in the semiclassical regime*, SIAM Journal on Scientific Computing, 25(2003), no. 1, 27-64.
[9] S. DATTA, *Electronic Transport in Mesoscopic Systems*, Cambridge University Press, 1995.
[10] S. DATTA, *Quantum Transport: Atom to Transistor*, Cambridge University Press, 2005.
[11] P. HARRISON, *Quantum wells, wires and dots: theoretical and computational physics of semiconductor nanostructures*, Jonh Wiley & Sons, New York, 2000.
[12] H.X. HUANG AND Z.L. LI, *Convergence analysis of the immersed interface method*, IMA Journal of Numerical Analysis, 19(1999), 583-608.
[13] T. JAHNKE AND C. LUBICH, *Error bounds for exponential operator splittings*, BIT, 40(2000), no. 4, 735-744.
[14] S. JIN, P. MARKOWICH AND C. SPARBER, *Mathematical and computational methods for semiclassical Schrödinger equations*, Acta Numerica, to appear in 2011.
[15] M.C. LAI AND Z.L. LI, *The immersed interface method for the Navier-Stokes equations with singular forces*, Journal of Computational Physics, 171(2001), 822-842.
[16] L. LEE AND R.J. LEVEQUE, *An immersed interface method for incompressible Navier-Stokes equations*, SIAM Journal on Scientific Computing, 25(2003), no. 3, 832-856.
[17] C. LENT AND D. KIRKNER, *The quantum transmitting boundary method*, Journal of Applied Physics, 67(1990), 6353-6359.
[18] R.J. LEVEQUE AND Z.L. LI, *The immersed interface method for elliptic equations with discontinuous coefficients and singular sources*, SIAM Journal on Numerical Analysis, 31(1994), no. 4, 1019-1044.
[19] R.J. LEVEQUE AND Z.L. LI, *Immersed interface method for Stokes flow with elastic boundaries or surface tension*, SIAM Journal on Scientific Computing, 18(1997), 709-735.
[20] Z.L. LI, *A note on immersed interface methods for three dimensional elliptic equations*, Computers & Mathematics with Applications, 31(1996), no. 3, 9-17.
[21] Z.L. LI, *A fast iterative algorithm for elliptic interface problems*, SIAM Journal on Numerical Analysis, 35(1998), no. 1, 230-254.
[22] Z.L. LI, *The immersed interface method using a finite element formulation*, Applied Numerical Mathematics, 27(1998), 253-267.
[23] Z.L. LI, *An overview of the immersed interface method and its applications*, Taiwanese Journal of Mathematics, 7(2003), no. 1, 1-49.
[24] Z.L. LI AND K. ITO, *Maximum principle preserving schemes for interface problems with discontinuous coefficients*, SIAM Journal on Scientific Computing, 23(2001), no. 1, 339-361.
[25] Z.L. LI AND A. MAYO, *ADI methods for heat equations with discontinuties along an arbitrary interface*, Proceedings of Symposia in Applied Mathematics, 48(1993), 311-315.
[26] T. LU AND W. CAI, *A Fourier spectral-discontinuous Galerkin method for time-dependent 3-D Schrödinger-Poisson equations with discontinuous potentials*, Journal of Computational and Applied Mathematics, 220(2008), 588-614.
[27] T. LU, W. CAI AND P.W. ZHANG, *Conservative local discontinuous Galerkin methods for time dependent Schrödinger equation*, International Journal of numerical analysis and Modeling, 2(2005), no. 1, 75-84.
[28] P.A. MARKOWICH, P. PIETRA AND C. POHL, *Numerical approximation of quadratic obaservables of*

Schrödinger-type equations in the semiclassical limit, Numerische Mathematik, 81(1999), no. 4, 595-630.

[29] P.A. MARKOWICH, P. PIETRA, C. POHL AND H.P. STIMMING, *A wigner-measure analysis of the Dufort-Frankel scheme for the Schrödinger equation*, SIAM Journal on Numerical Analysis, 40(2002), no. 4, 1281-1310.

[30] P.A. MARKOWICH, C. RINGHOFER AND C. SCHMEISER, *Semiconductor Equations*, Springer Verlag Wien, 1990.

[31] H. MIZUTA AND T. TANOU, *The Physics and Applications of Resonant Tunnelling Diodes*, Cambridge University Press, 1995.

[32] C.S. PESKIN, *The immersed boundary method*, Acta Numerica, 11(2002), 479-517.

[33] J. PIRAUX AND B. LOMBARD, *A new interface method for hyperbolic problems with discontinuous coefficients. One-dimensional acoustic example*, Journal of Computational Physics, 168(2001), 227-248.

[34] E. POLIZZI AND N. BEN ABDALLAH, *Subband decomposition approach for the simulation of quantum electron transport in nanostructures*, Journal of Computational Physics 202(2005), no. 1, 150-180.

[35] A.K. TORNBERG AND B. ENGQUIST, *Numerical approximations of singular source terms in differential equations*, Journal of Computational Physics, 200(2004), no. 2, 462-488.

[36] W. WANG AND C.W. SHU, *The WKB local discontinuous Galerkin method for the simulation of Schrödinger equation in a resonant tunneling diode*, Journal of Scientific Computing, 40(2009), no. 1-3, 360-374.

[37] C. WEISBUCH AND B. VINTER, *Quantum Semiconductor Structures: Fundamentals and Applications*, Academic Press, 1991.

[38] L.X. WU, *Dufort-Frankel-type methods for linear and nonlinear Schrödinger equations*, SIAM Journal on Numerical Analysis, 33(1996), no. 4, 1526-1533.

[39] H. WU, *High order scheme for Schrödinger equation with discontinuous potential II: novel methods for dynamic problems in the semiclassical regime*, in preparation.

[40] Y. XU AND C.W. SHU, *Local discontinuous Galerkin methods for nonlinear Schrödinger equations*, Journal of Computational Physics, 205(2005), 72-97.

[41] C.M. ZHANG AND R.J. LEVEQUE, *The immersed interface method for acoustic wave equations with discontinuous coefficients*, Wave Motion, 25(1997), 237-263.